PCCP

View Online
Dynamic Article Links

Cite this: *Phys. Chem. Chem. Phys.*, 2011, **13**, 14466–14475

www.rsc.org/pccp

PAPER

Interaction between NO and Na, O, S, Cl on Au and Pd(111) surfaces

Li-Yong Gan,[ab] Ren-Yu Tian,[a] Xiao-Bao Yang,[a] Song-Lin Peng[b] and Yu-Jun Zhao*[ab]

Received 30th March 2011, Accepted 11th May 2011
DOI: 10.1039/c1cp20974d

NO co-adsorption with X (X = Na, O, S, and Cl) on Au and Pd(111) surfaces is studied using density functional theory (DFT) calculations to get a deeper insight into the extraordinary sulfur enhanced adsorption on the Au surface. It is found that both electronegative and electropositive adatoms can enhance NO adsorption on Au(111). In Na + NO/Au(111), the strong electrostatic attraction between Na and NO dominates and stabilizes NO adsorption, though Na-induced surface negative charging weakens NO adsorption. In (O, S, Cl) + NO/Au, the electronegative atoms would induce a slight surface distortion and enhance NO adsorption accordingly. NO adsorption on Pd(111) is enhanced by Na, but weakened by electronegative species. We suggest that the unique features of noble metals, *i.e.*, *the narrow DOS at the Fermi level* (E_F) *and the deep buried d-band center*, should play an important role in the promotion of NO adsorption on their surface as the CO case.

1. Introduction

Nitrogen oxide species, NO_x, similar to carbon oxides, are common toxic air pollutants resulting from fossil fuel combustion. The conversion of NO_x to environmentally friendly gas is one of the most important processes in industry. In pursuit of new converters with more efficient catalytic reactivity, extensive efforts have been carried out to explore NO adsorption and dissociation on metal surfaces both experimentally[1–3] and theoretically,[4–8] and significant progress has been achieved. It has been found that top-site NO adsorption prefers to tilt away from the normal direction on transition metals (TMs) and noble metals with high *d*-band filling, while perpendicular top-site NO adsorption is more favorable[8] on TMs with low *d*-band filling. Meanwhile, due to the partial occupation in the anti-bonding $2\pi^*$ level, NO dissociation energy is 630 kJ mol^{-1}, which is much lower than that of CO (1076 kJ mol^{-1} in gas phase[5]). As a result, NO dissociation more readily occurs on the metal surfaces. It has been concluded that dissociative adsorption of NO is dominant on the surfaces of TMs with incomplete *d*-band filling, while molecular adsorption is more favorable on noble metal surfaces (*e.g.*, Pd and Pt).[5]

Gold (Au), once the noblest metal,[9] has recently earned a reputation as a potential green catalyst[10,11] due to its unexpectedly high catalytic performances, particularly the high catalytic selectivity[12–16] observed in well dispersed gold nanoparticles on reducible metal oxide supports. It is generally accepted that the low-coordinated sites may play a key role[17–22] for the high reactivity. Other factors, such as support interactions[23,24] and charge transfer,[25,26] may be also important. In addition, recent studies indicated that sulfur (S) containing species on Au surfaces can also exert several unexpected positive effects. For example, the presence of S could stabilize subsequent CO adsorption[27,28] and lower the H_2O dissociation barrier on Au(111).[29] It has been observed that room-temperature CO oxidation on Au/TiO_2 can be dramatically enhanced by the additive of sulfate ions.[30] The high catalytic performances along with the extraordinary novel phenomena greatly distinguish Au-based catalysts from other traditional TM catalysts.

Residual S containing species (often found as impurities in petroleum-derived chemical feedstocks and synthesis gas as well as automobile exhaust gas) have remarkably negative effects on the performance of the conventional catalysts.[31,32] It deactivates these catalysts after long-term operation, and causes considerable financial loss in the petrochemical and automobile industries.[33] Therefore, it is of significant importance to understand the interactions between S and reactive molecules, *i.e.* CO and NO. Co-adsorption of CO and S on metal surfaces has been well studied experimentally[34–38] and theoretically[28,39–41] on either mono- or bi-metal surfaces and a consensus has been reached that the poisoning effects of S on CO generally show a combination of steric (or structural) effects and electronic effects. Unfortunately, such knowledge is still rather limited on a microscopic level, especially for NO.

The interactions among different co-adsorbates on metal surfaces play an important role in heterogeneous catalysis because these may prefer/exclude a certain reaction pathway and give rise to a co-adsorption complex, which can either be a "promoter"[24,42–45] enhancing the reactivity and controlling

[a] *Department of Physics, South China University of Technology, Guangzhou 510640, P. R. China. E-mail: zhaoyj@scut.edu.cn; Fax: +86-20-87112837; Tel: +86-20-87110426*
[b] *State Key Laboratory of Physics and Chemistry of Luminescence, Guangzhou 510640, P. R. China*

the selectivity, or act as a "poisoner"[39,46–48] that reduces or even quenches the reaction rate adversely. These interactions may originate from different factors: direct overlap of wave functions, induced nonlocal dipole–dipole electrostatic interactions, indirect substrate metal *d*-bands, or a combination of several factors.[49] In our previous study of CO + X co-adsorption on Au,[50] we found that the pre-covered species (Na, O, S and Cl) induced charge effects that can shift the Au *d*-band upwards/downwards relative to the Fermi-level (E_F), stabilizing/destabilizing subsequent CO adsorption, respectively. NO is another common toxic air-pollutant besides CO. Are there any similar phenomena for NO co-adsorption compared to CO? Moreover, are there any common mechanisms that can be extended to X + NO/Au co-adsorption systems? Aiming at these two issues, we present extensive density functional theory (DFT) calculations to comparatively study NO adsorption on X pre-covered Au and Pd surfaces, in order to give an insight into the fundamental issues involved in heterogeneous catalysis and surface science.

2. Computational details

This work is conducted by the Vienna *Ab initio* Simulation Package (VASP)[51–54] with the frozen-core projector-augmented-wave (PAW) method.[55,56] The Perdew Wang (PW91) generalized gradient approximation (GGA)[57,58] functional is employed for the exchange–correlation energy. All the surfaces are modeled with a 5-layer slab with a vacuum thickness of 15 Å. The adsorbed species are put on one side of the slab.[59] The three uppermost layers are fully relaxed, while the two bottommost layers are fixed at their bulk structure with the previous optimized bulk lattice constants, 4.18 Å for Au and 3.96 Å for Pd.[28] A 3 × 3 supercell is used to simulate S as well as other adatoms X (X = Na, O, S and Cl) and NO co-adsorption on Au(111) and Pd(111) surfaces (shown in Fig. 1). A cutoff energy of 500 eV and a Monkhorst–Pack K-point sampling of 5 × 5 × 1 for each 3 × 3 surface unit cell are employed. The calculations, especially in the co-adsorption systems, are well converged with regard to energy cutoff and the K-point sampling. Higher values of energy cutoff (600 eV) and K-point sampling (7 × 7 × 1) vary the NO adsorption energy on S pre-adsorbed Au(111) less than 5 meV. The residual forces of each relaxed ion are less than 0.03 eV Å^{-1}. The frequencies are calculated with the fixed substrates and X, while only NO is allowed to vibrate in any direction at a displacement of 0.02 Å. The Wigner–Seitz radii for each element are r^{Au} = 1.503 Å, r^{Pd} = 1.434 Å, r^{Na} = 1.757 Å, r^{O} = 0.82 Å, r^{S} = 1.164 Å, r^{Cl} = 1.111 Å, r^{N} = 0.741 Å, respectively, for the projected density of states (PDOS) calculations. The positions of the *d*-band centers are calculated only considering the occupied states.

The co-adsorption energy of NO on X pre-adsorbed metal surfaces is defined as:

$$E_{ad} = -(E_{NO/X\text{-}M} - E_{X/M} - E_{NO}), \quad (1)$$

$E_{NO/X\text{-}M}$, $E_{X/M}$, and E_{NO} are the energies of NO and X co-adsorbed on metal (M = Au and Pd) surfaces, X pre-adsorbed on metal surfaces, and NO molecule in the gas phase, respectively.

In order to straighten out the interactions between X and NO on the two surfaces, the charge density differences in selected co-adsorption systems are depicted. Here, the charge density difference is calculated as

$$\Delta\rho = \rho_{X+NO/M(111)} - \rho_{X/M(111)} - \rho_{NO/M(111)} + \rho_{M(111)} \quad (2)$$

where $\rho_{X+NO/M(111)}$, $\rho_{X/M(111)}$, $\rho_{NO/M(111)}$, and $\rho_{M(111)}$ are the total charge densities of X + NO/M(111), X/M(111), NO/M(111), and the clean metal surfaces, respectively. The atom positions in each isolated system are identical to those in X + NO/M(111).

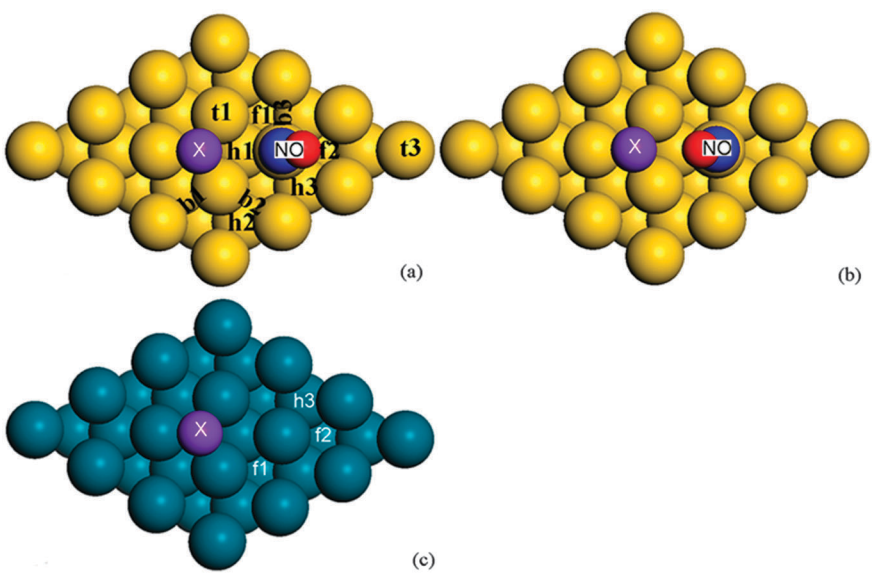

Fig. 1 (a), (b): Co-adsorption of NO and X on Au(111); (c): co-adsorption of NO and X on Pd(111). The letters t, b, f and h stand for atop, bridge, fcc and hcp sites, respectively, while 1, 2, and 3 indicate the first, second and third nearest site relative to the adatom X, respectively.

3. Results and discussions

3.1 NO adsorption on clean Au and Pd(111) surfaces

We investigated NO adsorption on the two prototype metal surfaces as a starting point, and the results are listed in Table 1. On Au(111), the most energetically favorable site is atop, not fcc, suggesting that the *d*-band filling may be an important factor but not the dominant one in NO adsorption on Au(111).[8] NO prefers the fcc site on the Pd(111) surface, while bridge site adsorption is unstable since NO would relax spontaneously to the nearby fcc sites as those on Pt(111).[60,61] The stretching frequencies of NO adsorption on the two metal surfaces are also calculated. On each metal surface, increasing coordination from atop to fcc weakens the N–O bond strength gradually, consistent with the change in the N–O bond length. This is because NO π-orbitals are more readily able to hybridize with TM $d_{xz,yz}$ states for NO at hollow sites. Charge transfer from metal to NO π-orbitals is facilitated, and therefore a more evident softening of N–O bond strength is found.[8] In addition, the N–O axis is tilting away from the surface normal direction at the top sites while perpendicular to the surface at the other adsorption sites on the two metal surfaces. These results are in good agreement with previous studies.[5,8,60,62]

3.2 NO adsorption on S pre-covered Au and Pd(111) surfaces

In S + NO/Au(111), the co-adsorption is modeled with S at an fcc hollow site and NO at various trial sites based on our previous study[28] [*cf*. Fig. 1(a)]. NO adsorption at t1, b1 and h1 are extremely unstable, and would relax spontaneously to the nearby sites. NO adsorption at the second nearest atop site (t2) on Au(111) is modeled with the N–O axis tilted away from S (labeled as Au–S_f + $NO_{t2}{}^a$) and towards S (labeled as Au–S_f + $NO_{t2}{}^b$) [*cf*. Fig. 1(a) and (b)] according to the results of NO adsorption on clean Au(111). On Pd(111), three different hollow sites (f1, h2, and f2) with respect to S are taken into account for NO while S is located at fcc, Fig. 1(c), allowing for the simulation for the long-range effect of S on the Pd surface.

It can be seen that the most energetically favorable configuration is NO at t2 site [*cf*. Fig. 1(a)] with its O portion away from the pre-adsorbed S atom. Meanwhile, the presence of S can stabilize NO adsorption in both Au–S_f + $NO_{t2}{}^a$ and Au–S_f + $NO_{t2}{}^b$, 0.54 and 0.39 eV, respectively, *vs*. 0.33 eV on clean Au(111). The smaller increase of NO adsorption energy in Au–S_f + $NO_{t2}{}^b$ is expected to be the result of a larger repulsion between O and S atoms than that in Au–S_f + $NO_{t2}{}^a$. On Pd(111), the presence of S drastically weakens the nearby NO adsorption. However, the destabilization of S on NO is rather local (*cf*. Table 2) in comparison with that on CO.[28] Meanwhile, the calculated N–O stretching frequencies on both S pre-covered metal surfaces are all blue-shifted with respect to those on the clean surfaces, especially for NO adsorption at h2 and f2 sites on S/Pd surface. This indicates that S poisoning is still a long-range effect though the N–Pd bond is affected locally by S. The existence of sulfur depletes surface active electrons even at the nonadjacent sites.[39] This is against charge transfer from substrates to NO 2π* anti-bonding states,[63] and consequently N–O bond is less weakened with respect to that on the clean surface.

Table 1 Adsorption energies, E_{ad}, N–O bond lengths, d_{N-O}, and stretching frequencies, *f*, of NO on Au and Pd(111). The experimental value in the gas phase is also listed in the brackets

	Site	E_{ad} (eV)	d_{N-O} (Å)	*f* (cm^{-1})
Gas phase	—	—	1.17	1905 [1903][a]
Au(111)	Top	0.33	1.17	1742
	Bridge	0.19	1.19	1641
	fcc	0.20	1.20	1571
	hcp	0.13	1.19	1599
Pd(111)	Top	1.52	1.18	1731
	Bridge	—	—	—
	fcc	2.35	1.21	1545
	hcp	2.30	1.21	1560

[a] Ref. 79.

Table 2 Adsorption energies, E_{ad}, bond lengths of N–O, d_{N-O}, angle between the N–O axis and the normal direction of the metal surfaces, $\alpha_{\perp\text{-NO}}$, and stretching frequencies, *f*, for NO adsorption on S pre-covered Au and Pd(111). The subscript letters and numbers are defined in Fig. 1

System	E_{ad} (eV)	d_{N-O}(Å)	$\alpha_{\perp\text{-NO}}$ (°)	*f* (cm^{-1})
Au–S_f + $NO_{t2}{}^a$	0.54	1.17	42.0	1751
Au–S_f + $NO_{t2}{}^b$	0.39	1.17	44.9	1747
Au–S_f + NO_{b2}	−0.01	1.18	11.7	—
Au–S_f + NO_{b3}	0.21	1.18	11.7	1661
Au–S_f + NO_{f1}	0.20	1.18	5.7	1638
Au–S_f + NO_{h3}	0.17	1.19	0.4	1622
Au–S_f + NO_{f2}	0.13	1.20	0.3	1575
Au–S_f + NO_{t3}	0.39	1.17	46.7	1741
Pd–S_f + NO_{f1}	2.01	1.21	5.3	1561
Pd–S_f + NO_{h3}	2.30	1.21	0.3	1568
Pd–S_f + NO_{f2}	2.35	1.21	0.6	1562

3.3 X adsorption on Au and Pd(111) surfaces

Before investigating the effects of X on NO adsorption, the properties of X adsorption are calculated. The most energetically preferred sites for O, S and Cl on the two surfaces are all fcc, while for Na, the three-fold hollow sites (fcc and hcp) are more energetically favorable and degenerate. Therefore, only the results of X at fcc are listed in Table 3. It is clear that the adsorption energies are in an increasing series of Na < Cl < O < S on both surfaces. Bader charge analysis[64] suggests that Na will donate its valence electron to TM surfaces once it adsorbs on the surfaces, a clear indication of an ionic characteristic.[42,65] For the three electronegative adatoms, the strongest bonded atom is sulfur, verifying that to remove S from the surface is hard once the surface is poisoned by S.

Table 3 Adsorption energies, E_{ad}, bond lengths of M–X (M = Au and Pd), d_{M-X}, and Bader charge analysis on X adatoms on M(111) surfaces

	X	E_{ad} (eV)	d_{M-X}	Charge (e)
Au–X–fcc	Na	2.27	2.942	+0.993
	O	3.40	2.144	−0.787
	S	3.63	2.409	−0.358
	Cl	2.40	2.674	−0.408
Pd–X–fcc	Na	2.51	2.884	+0.990
	O	4.75	2.005	−0.793
	S	5.04	2.251	−0.230
	Cl	3.19	2.455	−0.404

O atom accumulates the most electrons, manifesting the most ionic characteristics. The S atom accepts the least electrons, displaying the most covalent feature. The charge difference may result from their corresponding Pauling's electronegativity: O (3.44) > Cl (3.16) > S (2.58). The calculated adsorption energies and bond lengths of O, S, and Cl on the two metal surfaces agree well with previous experimental[66–70] and theoretical studies.[28,71–73]

3.4 NO adsorption on X pre-covered Au and Pd(111) surfaces

It has been observed above that S can enhance NO adsorption on Au(111). Then, can the observation extend to other NO co-adsorption systems? If the answer is yes, is there any difference between NO and CO? We have subsequently studied NO adsorption on Na, O and Cl pre-covered Au surfaces to clarify these questions. Analogous calculations on Pd(111) are also conducted for comparison. The co-adsorption of X + NO on the two surfaces is intuitively modeled with X at an fcc hollow site on both surfaces and NO at t2 (f1) on Au (Pd) according to the results of NO + S/Au(111) and NO + S/Pd(111). Similarly, the two tilting directions of N–O are all taken into account for X + NO/Au(111), *i.e.*, tilting away from X ($Au–X_f + NO_{t2}^{a}$) and towards X ($Au–X_f + NO_{t2}^{b}$), as shown in Fig. 1. NO adsorption on charged metal substrates has also been calculated, and the results are tabulated in Table 5. It is found that positively/negatively charged Au(111) also stabilizes/destabilizes NO adsorption due to the charge effects,[50] while the charge effect does not exert much influence on NO adsorption on Pd(111). Convergence for NO adsorption on charged Au surfaces has been carefully tested with regard to the slab layers and vacuum thickness.[74] Additionally, we have also checked NO adsorption with either the N or O atom directly approaching Na. However, the molecular adsorption is extremely unstable on both surfaces, and the dissociative adsorption was not obtained, either. The binding energies of Na atom with substrates and with a single NO molecule are comparatively calculated to ascertain the mechanism. The binding energies are 2.27 and 2.51 eV for Na on Au and Pd, respectively, which are much larger than with a single NO molecule, 0.96 eV. This indicates that the Na adatom is still prone to bonding with the substrate rather than with NO molecule directly as NO is introduced to the Na pre-adsorbed systems.

3.4.1 NO interaction with X on Au(111) surfaces. Contrary to the destabilization effect of Na in the Na + CO/Au system,[50] Na plays a promotional role in Na + NO/Au, stabilizing neighboring NO adsorption. Bader[64] charge analysis for $Au–Na_f + NO_{t2}^{b}$ shows that Na and NO accumulates positive and negative charges with Na containing +1.000 and NO −0.356*e* (+0.760*e* for N and −1.116*e* for O), respectively. NO is tilting towards Na, with the angle between the normal of the surface and N–O axis of 51.9°, which is larger than 47.5°, that are on clean Au(111), facilitating the approach of O towards Na. The O–Na distance is 2.17 Å, much shorter than that of N–Na, 2.43 Å. These parameters are over 1 Å shorter than the corresponding values in Na + CO/Au where CO adsorption is destabilized. Thus, one can expect a much stronger Coulomb attraction between Na and NO than that between Na and CO in the corresponding co-adsorption system. Consequently, NO adsorption at t2 on Na/Au(111) is enhanced due to the overall Coulomb attraction, despite that the negative charge weakens NO adsorption, 0.21 eV *vs.* 0.33 eV on neutral Au(111).

From Table 4, it can be seen that all the studied electronegative adatoms can stabilize subsequent NO adsorption at t2 site on Au. The most enhancement for NO adsorption is found on S/Au(111), while for CO is on O/Au(111).[50] As listed in Table 3, the O adatom accumulates charges almost twice as much as S does, and results in a more notable induced charge effect. The calculated *d*-band center of Au atom bonded to NO in O/Au(111) is higher than that in S/Au(111), −3.38 eV *vs.* −3.43 eV. Here, a simple local *d*-band model fails to explain the trend of NO adsorption on X/Au(111).

To explore the interactions between co-adsorbates on Au(111), charge density difference plots of NO adsorption on Na, O and S pre-covered Au surfaces in relatively stable configuration are illustrated in Fig. 2. A charge difference plot of $Au–Na_f + NO_{t2}^{a}$ is also presented in Fig. 2(b) to understand the unlikely enhancement of NO adsorption since both Na and N atoms are positively charged. The charge density

Table 4 Adsorption energies, E_{ad}, structural parameters, and N–O bond stretching frequencies, *f*, Bader charge analysis on X, NO for NO adsorption on X/Au(111) and X/Pd(111). Distances between X and N, $d_{X–N}$; distances between X and O, $d_{X–O}$; bond lengths of NO, $d_{N–O}$. Only structural parameters, frequencies and charges for relatively more stable co-adsorption configuration are listed. The subscript letters and numbers are defined in Fig. 1

System	E_{ad} (eV)	$d_{X–N}$ (Å)	$d_{X–O}$ (Å)	$d_{N–O}$ (Å)	*f* (cm^{-1})	Charge of X (e)	Charge of NO (e)
$Au–NO_t$	0.33	—	—	1.17	1742	—	−0.047
$Au–Na_t + NO_{t2}^{a}$	0.40	—	—	—	—	—	—
$Au–Na_f + NO_{t2}^{b}$	0.44	3.29	2.43	1.21	1522	+1.000	−0.356
$Au–O_f + NO_{t2}^{a}$	0.45	3.19	4.28	1.17	1755	−0.803	−0.002
$Au–O_f + NO_{t2}^{b}$	0.39	—	—	—	—	—	—
$Au–S_f + NO_{t2}^{a}$	0.54	3.11	4.12	1.17	1751	−0.337	−0.020
$Au–S_f + NO_{t2}^{b}$	0.39	—	—	—	—	—	—
$Au–Cl_f + NO_{t2}^{a}$	0.40	3.10	4.09	1.17	1755	−0.407	−0.017
$Au–Cl_f + NO_{t2}^{b}$	0.36	—	—	—	—	—	—
$Pd–NO_f$	2.34	—	—	1.21	1545	—	−0.491
$Pd–Na_f + NO_{f1}$	2.45	2.89	2.46	1.25	1366	+0.996	−0.731
$Pd–O_f + NO_{f1}$	2.08	3.11	3.45	1.21	1567	−0.812	−0.430
$Pd–S_f + NO_{f1}$	2.01	3.26	3.49	1.21	1561	−0.286	−0.434
$Pd–Cl_f + NO_{f1}$	2.14	3.37	3.43	1.21	1564	−0.398	−0.418

Table 5 Adsorption energies, E_{ad} (eV), N–O bond lengths, d_{N-O} (Å) for NO on charged Au^{δ} and Pd^{δ} surfaces (δ = 2−, 1−, 1+, and 2+), and Bader charge analysis on the metal atoms bonded to NO. Au^0 and Pd^0 indicate neutral metal surfaces. The subscript letters "t" and "f" stand for adsorption sites, atop and fcc, respectively

System	E_{ad} (eV)	d_{N-O} (Å)	Charge (e)
Au^0–NO_t	0.33	1.17	−0.018
Au^{1+}–NO_t	0.65	1.16	+0.013
Au^{2+}–NO_t	1.04	1.14	+0.038
Au^{1-}–NO_t	0.21	1.19	−0.055
Pd^0–NO_f	2.34	1.21	−0.029
Pd^{1+}–NO_f	2.45	1.20	+0.009
Pd^{2+}–NO_f	2.62	1.19	+0.052
Pd^{1-}–NO_f	2.30	1.22	−0.067
Pd^{2-}–NO_f	2.29	1.23	−0.104

difference of NO on clean Au(111) is also shown as a reference. For NO adsorption at the top site of clean Au(111), the 1π states of NO are clearly split (not shown), in sharp contrast to those on other TMs.[8] From charge density difference contours, it is clear that electrons deplete in NO 5σ and Au d_{z^2} states but accumulate in NO 2π* states and the bonding region between NO and Au [*cf.* Fig. 2(a)]. This shows that the interaction between NO and Au also corresponds to the donation and back-donation process.[63] In Au–Na_f + $NO_{t2}{}^b$ [*cf.* Fig. 2(b)†], electrons clearly accumulate in NO 2π* anti-bonding states. This is responsible for the weakness of N–O bond strength. The calculated NO stretching frequency is 1522 cm^{-1}, 220 cm^{-1} less than that on the clean Au(111). Furthermore, a pronounced polarization in NO 2π* states can be observed in O portion. Such a short distance of O–Na combined with the induced polarization in the NO molecule suggests that the ionic bonding trend between $Na^{\delta+}$ and $O^{\delta-}$ seems to be more dominant than the simple attractive interaction between $Na^{\delta+}$ and the whole $NO^{\delta-}$ molecule. In Au–Na_f + $NO_{t2}{}^a$, the attraction between Na and NO still prevails. In the charge difference contours [*cf.* Fig. 2(b)], one can see that Na induces a notable polarization at N portion in NO 2π* states. In addition, Na atom slightly approaches to NO with respect to its original adsorption site (*i.e.* the ideal fcc site), indicative of the attraction. The Na–Au bond lengths are all 2.94 Å before NO adsorption and change to 3.02, 2.96 and 2.96 Å after NO adsorption.

However, for NO co-adsorption with S and O, the situation is more complex. The charge density difference plots show that both S and O adatoms deplete charges in NO 2π* states, demonstrated at the N portion. Thus, the stretching frequencies of NO on S and O pre-covered Au(111) both experience a blue shift (*cf.* Table 4). As for S and O atoms themselves, charge depletion and accumulation can be seen in their p_z and p_x (p_y) orbitals, respectively, especially for O. By comparing the two co-adsorption systems, one can see that more electrons are accumulated at Au-d_{z^2} and the NO–Au bonding region in S + NO, demonstrating a relatively indirect interaction between S and NO through Au *d*-states. In O + NO, the N atom approaches the neighboring O adatom, and charge accumulation can be found between the adatom O and N atom of NO. These features reveal a more direct interaction between O and NO. Meanwhile, NO adsorption on positively charged Au surfaces is still favorable with respect to that on neutral Au surface. Briefly, there is not a general or dominant factor accounting for all the NO stabilization on X pre-covered Au surfaces, but it is rather case by case. For instance, interactions *via* indirect metal *d*-bands dominate in S + NO/Au and charged Au cases, while relatively direct electrostatic attraction and bonding trend are found primary in Na + NO/Au and O + NO/Au. The nature of the interactions between NO and X is different from those between CO and X, which will be further discussed in the final section.

3.4.2 NO interaction with X on Pd(111) surfaces. NO co-adsorption with Na, O, and Cl on Pd(111) is also studied for comparison, and the adsorption configurations are shown in Fig. 1(c). It can be seen that NO adsorption energy is increased and decreased at the nearby f1 site on Na and O (Cl) pre-adsorbed Pd(111), respectively. In order to explore the effects of electronegative and electropositive species, the PDOS (Fig. 3) and charge density difference plots (Fig. 4) of these systems are compared, and the corresponding plot of NO/Pd(111) is also shown for reference. The effect of electronegative adatoms is exemplified by NO adsorption on S/Pd surface.

The PDOS [*cf.* Fig. 3(d)] indicates the Na adatom shifts NO 2π* downwards, leading to a further occupation of NO 2π*, thus weakening the N–O bond strength. The calculated bond lengths and stretching frequencies are 1.25 Å, 1366 cm^{-1} and 1.21 Å, 1545 cm^{-1} with and without Na, respectively. Meanwhile, the presence of Na introduces a remarkable decrease in the NO 5σ and 1π molecular orbitals around −8 eV below E_F, which hybridize with Pd *d*-states, suggesting that the NO and Pd interaction is weakened. Nevertheless, the Na atom induces a notable polarization in NO 2π* states, giving rise to a strong electronegative attraction[75] between Na and NO, and therefore enhancing NO adsorption. Such big polarization at the O portion in the NO molecule also suggests that the ionic bonding trend between $Na^{\delta+}$ with $O^{\delta-}$ seems to be more dominant than the simple attraction between $Na^{\delta+}$ and the whole $NO^{\delta-}$ molecule.

In contrast, the electronegative adatoms (O and Cl) still destabilize NO adsorption as expected (*cf.* Table 4). In S + NO/Pd(111), a tiny peak can be observed in the PDOS of S atom around −8 eV below E_F, where NO 1π orbital locates, implying a direct interaction between NO and S. Meanwhile, the presence of S evidently decreases NO 5σ and 1π peaks. Apparent charge density depletions can be observed in NO 2π* orbital and NO-Pd bonding region [*cf.* Fig. 4(c)] at the same time. The features are responsible for the blue shift of N–O stretching mode and the decrease of NO adsorption because NO and S bond directly to the same Pd atom, resulting in a big repulsion due to the bonding competition.

Finally, it is interesting to mention the charge variations of X and NO before and after co-adsorption on both surfaces. From Table 4, it can be seen that upon NO adsorption Na atoms are further ionized, facilitating charge accumulation in NO molecules, while O and S gain electrons further, depleting electrons in NO with respect to that on clean surfaces. In Cl + NO, Cl atoms lose more or less electrons while remarkable depletion can also be found in NO molecules.

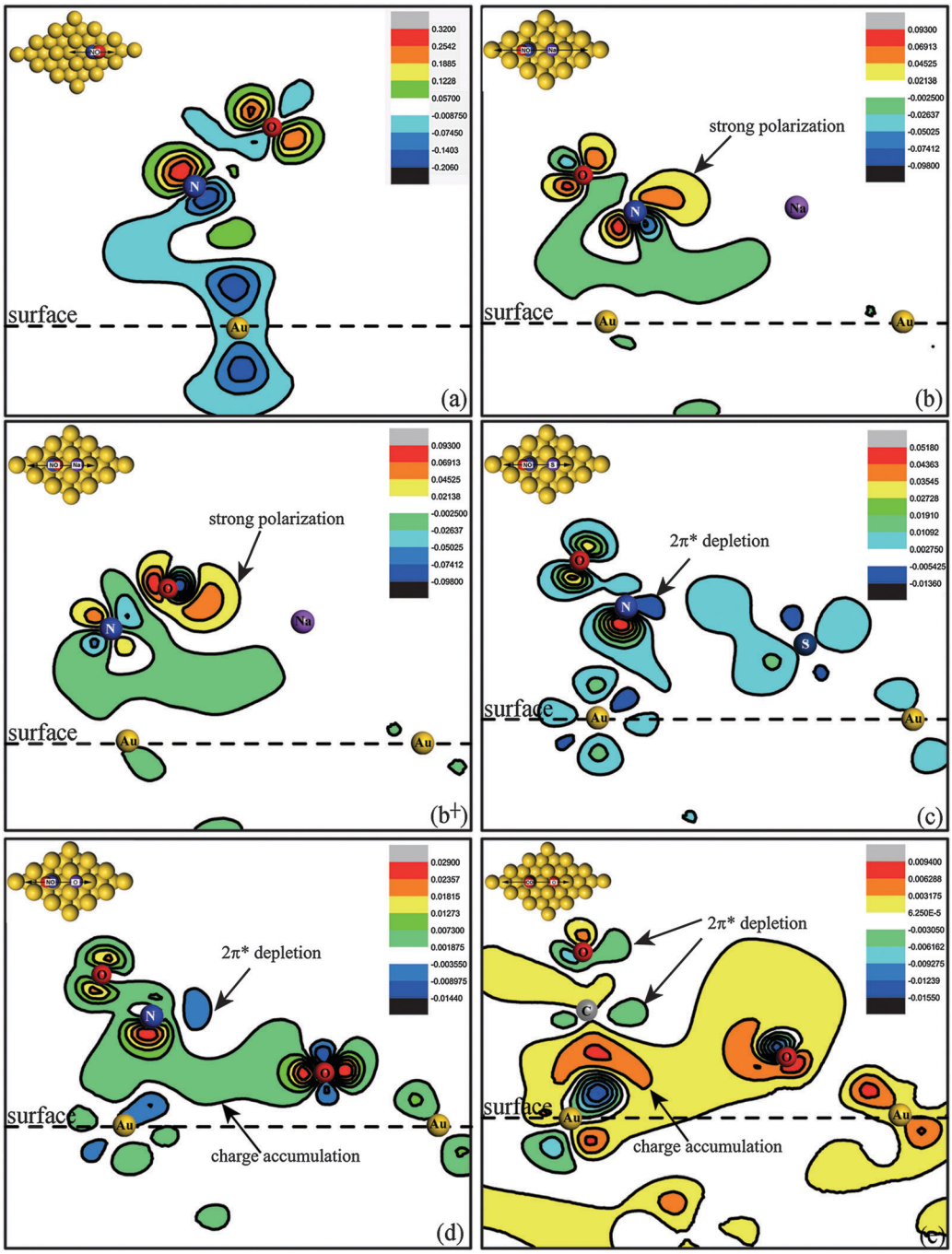

Fig. 2 Charge density difference plots: (a) Au–NO_t; (b) Au–Na_f + NO_{t2}[a]; (b†) Au–Na_f + NO_{t2}[b]; (c) Au–S_f + NO_{t2}[a]; (d) Au–O_f + NO_{t2}[a]; (e) Au–O_f + CO_{t2}. The cutting plane is shown in the upper left corner of each panel. Red and blue contours correspond to charge accumulation and depletion, respectively.

3.4.3 Further explanation for the different behaviors of $X^\dagger$ + NO and $X^\dagger$ + CO interaction on Au(111) ($X^\dagger$ = O, S and Cl). As shown above, the *d*-band center of O/Au is higher than that of S/Au, yet the NO adsorption energy experiences more increment on S/Au than on O/Au. Moreover, it has been shown that the interactions between the electronegative atom $X^\dagger$ and NO are complicated without a general or dominant contribution accounting for all the stabilization effects. As a result, the simple local *d*-band model can not well describe the trend of NO adsorption on $X^\dagger$/Au(111) since it neglects the *direct* interactions between co-adsorbates. The behavior of NO chemisorption on $X^\dagger$/Au, however, may be understood through the bond order conservation (BOC) concept,[61] in which the total bond order of all interacting two-center bonds is conserved and an overall consideration of various factors in a many-body system is concerned. In $X^\dagger$ + NO/Au systems, we treat the group of the first (Au1), second (Au2) nearest Au atoms relative to $X^\dagger$ and the subsequent adsorbing NO as an entity. According to BOC, the summation of bond order for $X^\dagger$–Au1, Au1–Au2 and NO–Au2 bonds should be conserved

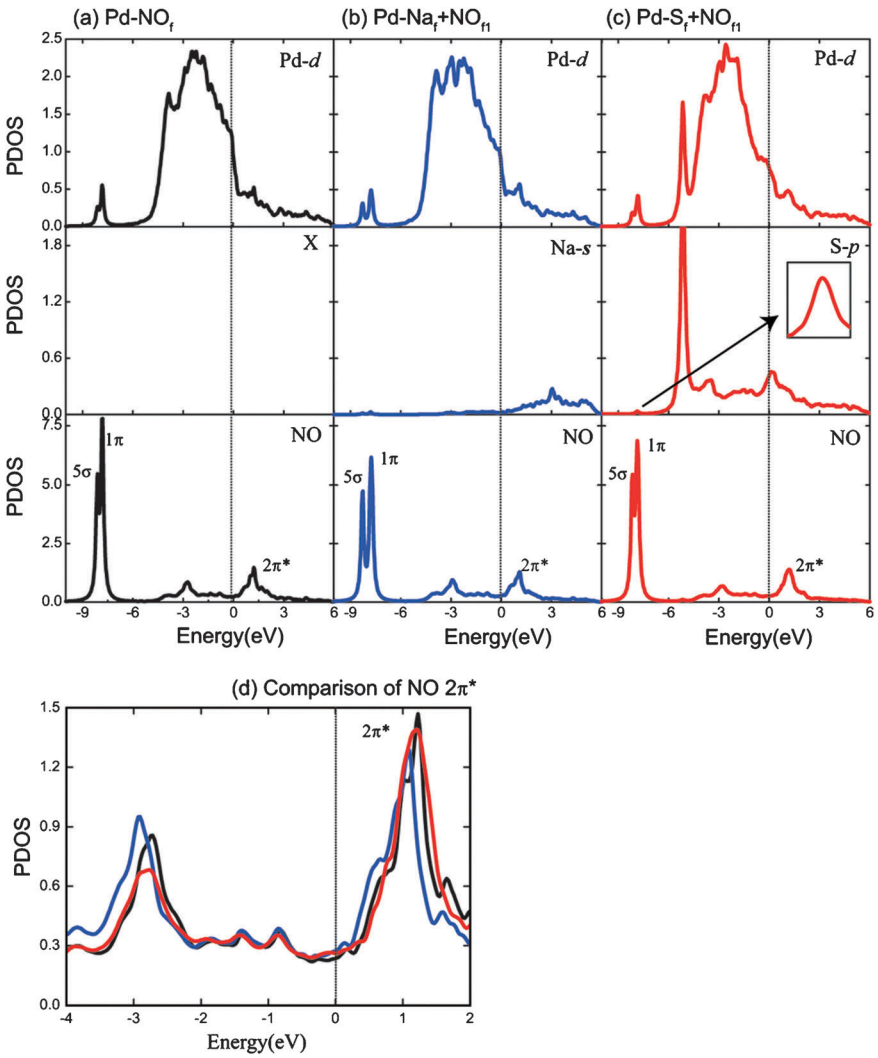

Fig. 3 *d*-Projected density of states (PDOS): (a) Pd–NO$_f$; (b) Pd–Na$_f$ + NO$_{f1}$; (c) Pd–S$_f$ + NO$_{f1}$; (d) comparison of NO 2π* orbital in Pd–NO$_f$, Pd–Na$_f$ + NO$_{f1}$ and Pd–S$_f$ + NO$_{f1}$. Black, blue, and red lines indicate NO adsorption on clean, Na pre-covered, and S pre-covered Pd(111), respectively. In the co-adsorption systems, Pd atoms projected are those that both NO and X bond to. E_F is set to zero.

in the X† + NO/Au(111). The Au1–Au2 bond strength can be characterized by the vacancy formation energy (E_f^{vac})[76] of Au2 as well as the Au1–Au2 bond length to some extent. Therefore, E_f^{vac} of Au2 upon X† adsorption[77] along with the Au1–Au2 bond length in X†/Au(111) and clean Au(111) as well as X†/Pd(111) and Pd(111) are calculated.

Table 6 indicates that E_f^{vac} of Au2 in X†/Au increases along S < O < Cl, suggesting that the bond order of Au1–Au2 in S/Au is the weakest. Therefore, as predicted by the BOC concept, the bond order of subsequent NO–Au2 should be the strongest. Our results show that NO adsorption energy on S/Au is 0.54 eV, greater than that on O/Au, Cl/Au and clean Au(111). At the meantime, the vacancy formation energies of Au2 correspond well with the bond lengths of Au1–Au2 variations. The longer the Au1–Au2 bond length is, the weaker the Au1–Au2 bond strength, and *vice versa*. Therefore, the change of the bond length of Au1–Au2 upon X† adsorption can be regarded as a simple scoreboard of the effect on the adsorption strength of NO on Au(111).

Instead, the *d* bands of Pd are often extended to the E_F, which will push up the DOS at E_F[49,50] As a result, it will form extremely strong covalent bonds with the pre-adsorbed electronegative atoms through their *d*-bands, and the *d*-band center shifts down evidently with its width increasing accordingly and the DOS at the E_F decrease substantially. Despite the elongation of Pd1–Pd2 bond length by electronegative X†, the poisoning effects still prevail, and thus weaken NO adsorption. The low DOS at E_F and the deeply buried *d*-band center of Au screen X† poisoning effects effectively. Thus, X†-induced promoting effects become dominant and stabilize NO adsorption.

Subsequently, we would like to compare NO and CO adsorption on X†/Au. We pointed out that the extraordinary S enhancement of CO adsorption originated from the induced positive charge effects in a previous study.[50] The more positive the Au atom is, the higher its *d*-band is relative to E_F, and the stronger CO adsorption will be. It was observed that the increment of the CO adsorption energy decreases along O > Cl > S. In the X† + NO/Au case, however, the order

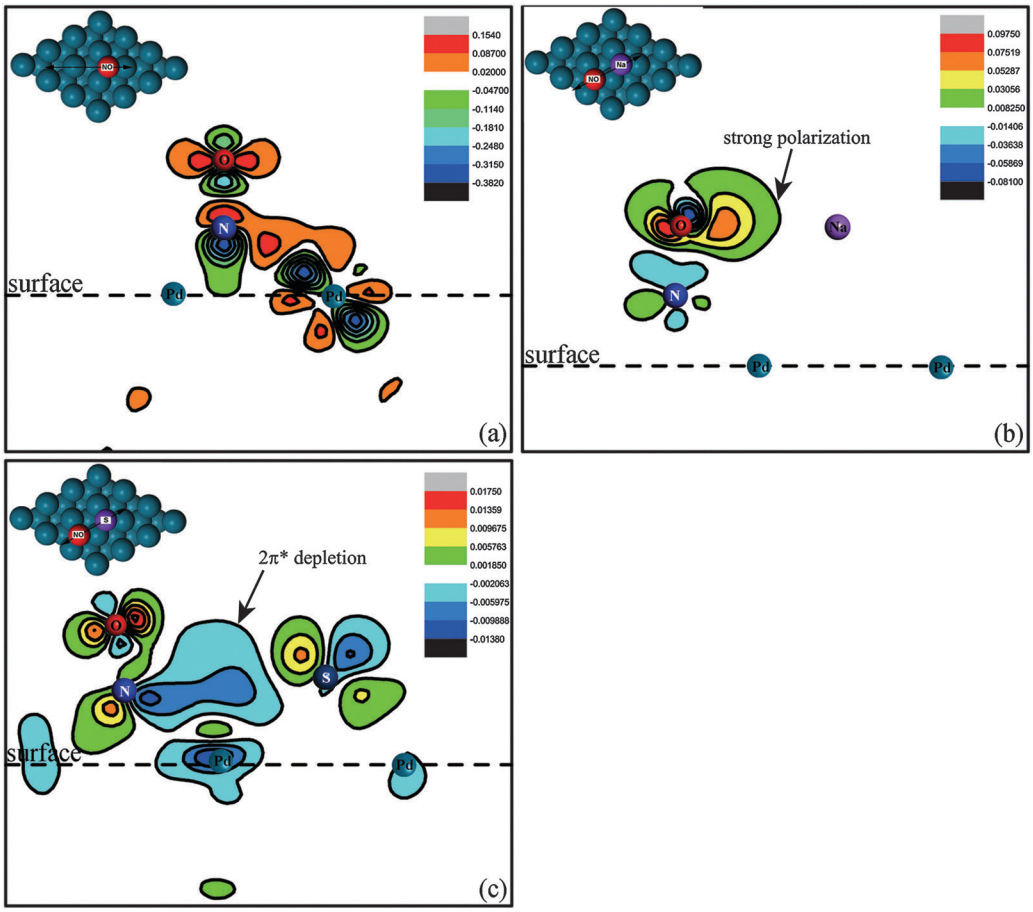

Fig. 4 Charge density difference plots: (a) Pd–NO_f; (b) Pd–Na_f + NO_{f1}; (c) Pd–S_f + NO_{f1}. The cutting plane is shown in the upper left corner of each panel. Red and blue contours correspond to charge accumulation and depletion, respectively.

Table 6 Bond lengths between the first and the second nearest metal atoms, d_{M1-M2}, with respect to X on the two metal surfaces, and the vacancy formation energies of M2, E_f^{vac}. The vacancy formation energy is calculated as $E_f^{vac} = E_{vac} + E_{bulk} - E_{surface}$, where E_{vac}, E_{bulk}, and $E_{surface}$ are the total energy of the surface with vacancy, the bulk metal atom, and metal (111) with and without O, S and Cl, respectively

System	d_{M1-M2} (Å)	E_f^{vac} (eV)
Au–Clean-surface	2.953	0.66
Au–O-fcc	2.987	0.41
Au–S-fcc	2.993	0.36
Au–Cl-fcc	2.979	0.44
Pd–Clean-surface	2.800	1.00
Pd–O-fcc	2.820	0.83
Pd–S-fcc	2.821	0.80
Pd–Cl-fcc	2.816	0.85

changes to S > O > Cl. Comparatively, the charge density difference plot of O + CO/Au is shown in Fig. 2(e). An obvious charge accumulation can be found in the CO and Au bonding region, indication of an indirect O–CO interaction through Au *d*-bands, while a direct interaction trend between O and NO is evident in O + NO/Au, suggesting that $X^{\dagger}$-induced charge effects influence CO adsorption indirectly *via* Au *d*-bands in $X^{\dagger}$ + CO/Au. Then, what is the origin of the difference? We argue that the different behaviors may be attributed to the difference between their adsorption structures: firstly, NO adsorption at the top site on $X^{\dagger}$/Au is tilting with N atom approaching $X^{\dagger}$ and O away from $X^{\dagger}$, while CO adsorption is almost perpendicular to the surface; secondly, N atom is not directly right on top of the Au atom, but slightly off, while the C atom is almost right on the top. The tilting configuration of NO brings it a nonlocal influence, which may extend to a certain degree, while the perpendicular structure makes CO influenced mainly by the adjacent Au atom. Consequently, the respective adsorption structure results in corresponding interactions stated above. By the way, it is found that NO adsorption is also enhanced on $X^{\dagger}$/Ag surfaces with the same order as that on $X^{\dagger}$/Au. NO adsorption energy (E_{ad}) on positively charged Ag surface can be increased to as large as 1.04 eV too. This may explain the contradiction between the large E_{ad} observed in experiment and extremely low E_{ad} obtained by DFT calculation.[5,78]

On conventional TM catalysts (Pd, Pt), the presence of sulfur-containing species would lower their *d*-band center and substantially reduce the DOS near the Fermi level, causing remarkably negative effects. Yet for the Au surface, its *d*-band is buried so deep and the DOS at E_F is so narrow that pre-adsorbed adatoms hardly influence these features, and other induced effects (*i.e.* charge effects, adsorbate–adsorbate electrostatic interaction) prevail and enhance NO adsorption.

Consequently, we would like to emphasize that the features of Au, *narrow DOS at E_F and deep buried d-band center*, should play an important role in the enhancement of subsequent NO as well as CO adsorption. Our unique findings of sulfur-enhanced adsorption on the noble metals may someday be instructive to the pursuit of new catalysts with high sulfur resistance, coupled with further studies on the subsequent reactions.

4. Summary

By the first-principles study, we find that both the pre-adsorbed electronegative species (*e.g.*, O, S, and Cl) and the electropositive atom (*e.g.*, Na) can enhance the neighboring NO adsorption *on Au(111) surface*. The promotion effect of Na can be ascribed to the strong Coulomb attraction between Na and NO, while the enhancement of NO adsorption by the electronegative atoms decreases along the series S > O > Cl, leading to a difficulty for a simple *d*-band center explanation mainly because it neglects the direct interactions between co-adsorbates. These, however, may be described by the bond order conservation concepts. *On Pd(111) surface*, NO adsorption is enhanced by the pre-adsorbed Na, but degraded by the pre-adsorbed electronegative species (O, S, Cl). The decrease of NO adsorption energy by O, S, Cl is found be the local bonding competition, while their poisoning effects still extend to a long range. Na atom enhances NO adsorption more likely through the ionic bonding trend between $Na^{\delta+}$ with $O^{\delta-}$ rather than the simply attractive interaction between $Na^{\delta+}$ and $NO^{\delta-}$. Conclusively, it is found that the features of *d* bands of Au, *i.e.*, *narrow DOS at E_F and deep buried d-band center*, play a vital role in the enhancement of NO and CO adsorption, which may provide potential guidance in the Au-based catalysis design.

Acknowledgements

This work is supported by MOST under project 2010CB631302, and the Fundamental Research Funds for the Central Universities, SCUT, under project 2009ZZ0068, 2009ZM0165, and 2011ZG0017, and completed with the cooperation of HPC Lab, Shenzhen Institute of Advanced Technology, CAS, China.

References

1 M. Bertolo and K. Jacobi, *Surf. Sci.*, 1990, **226**, 207–220.
2 W. A. Brown and D. A. King, *J. Phys. Chem. B*, 2000, **104**, 2578–2595.
3 P. J. Chen and D. W. Goodman, *Surf. Sci.*, 1993, **297**, L93–L99.
4 R. Burch, S. T. Daniells and P. Hu, *J. Chem. Phys.*, 2002, **117**, 2902–2908.
5 M. Gajdos, J. Hafner and A. Eichler, *J. Phys.: Condens. Matter*, 2006, **18**, 13–40 and references therein.
6 M. Gajdos, J. Hafner and A. Eichler, *J. Phys.: Condens. Matter*, 2006, **18**, 41–54.
7 Z. H. Zeng, J. L. F. Da Silva and W. X. Li, *Phys. Rev. B: Condens. Matter Mater. Phys.*, 2010, **81**, 085408.
8 Z. H. Zeng, J. L. F. Da Silva and W. X. Li, *Phys. Chem. Chem. Phys.*, 2010, **12**, 2459–2470.
9 M. Haruta, T. Kobayashi, H. Sano and N. Yamada, *Chem. Lett.*, 1987, 405–408.
10 C. H. Christensen and J. K. Nøskov, *Science*, 2010, **327**, 278–279.
11 A. Wittstock, V. Zielasek, J. Biener, C. M. Friend and M. Baumer, *Science*, 2010, **327**, 319–322.
12 M. Haruta, T. Kobayashi, H. Sano and N. Yamada, *Chem. Lett.*, 1987, **2**, 405–408.
13 A. K. Sinha, S. Seelan, S. Tsubota and M. Haruta, *Top. Catal.*, 2004, **29**, 95–102.
14 M. D. Hughes, Y. J. Xu, P. Jenkins, P. McMorn, P. Landon, D. I. Enache, A. F. Carley, G. A. Attard, G. J. Hutchings, F. King, E. H. Stitt, P. Johnston, K. Griffin and C. J. Kiely, *Nature*, 2005, **437**, 1132–1135.
15 T. Ishida and M. Haruta, *Angew. Chem., Int. Ed.*, 2007, **46**, 7154–7156.
16 B. Jorgensen, S. E. Christiansen, M. L. D. Thomsen and C. H. Christensen, *J. Catal.*, 2007, **251**, 332–337.
17 N. Lopez and J. K. Nøskov, *J. Am. Chem. Soc.*, 2002, **124**, 11262–11263.
18 N. Lopez, T. V. W. Janssens, B. S. Clausen, Y. Xu, M. Mavrikakis, T. Bligaard and J. K. Nøskov, *J. Catal.*, 2004, **223**, 232–235.
19 Z. P. Liu, P. Hu and A. Alavi, *J. Am. Chem. Soc.*, 2002, **124**, 14770–14779.
20 S. K. Shaikhutdinov, R. Meyer, M. Naschitzki, M. Baumer and H. J. Freund, *Catal. Lett.*, 2003, **86**, 211–219.
21 C. Lemire, R. Meyer, S. Shaikhutdinov and H. J. Freund, *Angew. Chem., Int. Ed.*, 2004, **43**, 118–121.
22 B. K. Min, X. Deng, D. Pinnaduwage, R. Schalek and C. M. Friend, *Phys. Rev. B: Condens. Matter Mater. Phys.*, 2005, **72**, 121410(R).
23 G. C. Bond and D. T. Thompson, *Gold Bulletin*, 2000, **33**, 41–51.
24 A. Bongiorno and U. Landman, *Phys. Rev. Lett.*, 2005, **95**, 106102.
25 B. Yoon, H. Hakkinen, U. Landman, A. S. Worz, J. M. Antonietti, S. Abbet, K. Judai and U. Heiz, *Science*, 2005, **307**, 403–407.
26 Z.-P. Liu, S. J. Jenkins and D. A. King, *Phys. Rev. Lett.*, 2005, **94**, 196102.
27 T. F. Zhang, Z. P. Liu, S. M. Driver, S. J. Pratt, S. J. Jenkins and D. A. King, *Phys. Rev. Lett.*, 2005, **95**, 266102.
28 L. Y. Gan, Y. X. Zhang and Y. J. Zhao, *J. Phys. Chem. C*, 2010, **114**, 996–1003.
29 L. Q. Xue, X. Y. Pang and G. C. Wang, *J. Phys. Chem. C*, 2007, **111**, 2223–2228.
30 P. Mohapatra, J. Moma, K. M. Parida, W. A. Jordaan and M. S. Scurrell, *Chem. Commun.*, 2007, 1044–1046.
31 J. K. Lee and H. K. Rhee, *J. Catal.*, 1998, **177**, 208–216.
32 J. Oudar and H. Wise, *Deactivation and Poisoning of Catalysts*, Dekker, New York, 1991.
33 J. A. Rodriguez and J. Hrbek, *Acc. Chem. Res.*, 1999, **32**, 719–728.
34 W. Erley and H. Wagner, *J. Catal.*, 1978, **53**, 287–294.
35 D. W. Goodman and *IUCCP Conference*, Texas A&M University, Texas, 1984.
36 D. W. Goodman and C. H. F. Peden, in *Proceedings of the Symposium on the Surface Science of Catalysts*, ed. M. L. Devinny and J. L. Gland, Philadelphia American Chemical Society, Washington, DC, 1984.
37 X. F. Hu and C. J. Hirschmugl, *Phys. Rev. B: Condens. Matter Mater. Phys.*, 2005, **72**, 205439.
38 K. Habermehl-Ćwirzeń and J. Lahtinen, *Surf. Sci.*, 2004, **573**, 183–190.
39 P. J. Feibelman and D. R. Hamann, *Phys. Rev. Lett.*, 1984, **52**, 61–64.
40 C. J. Zhang, P. Hu and M. H. Lee, *Surf. Sci.*, 1999, **432**, 305–315.
41 E. Wimmer, C. L. Fu and A. J. Freeman, *Phys. Rev. Lett.*, 1985, **55**, 2618.
42 Z. P. Liu and P. Hu, *J. Am. Chem. Soc.*, 2001, **123**, 12596–12604.
43 J. J. Mortensen, B. Hammer and J. K. Nøskov, *Phys. Rev. Lett.*, 1998, **80**, 4333–4336.
44 T. S. Kim, J. Gong, R. A. Ojifinni, J. M. White and C. B. Mullins, *J. Am. Chem. Soc.*, 2006, **128**, 6282–6283.
45 R. A. Ojifinni, N. S. Froemming, J. Gong, M. Pan, T. S. Kim, J. M. White, G. Henkelman and C. B. Mullins, *J. Am. Chem. Soc.*, 2008, **130**, 6801–6812.
46 C. H. Bartholomew, *Appl. Catal., A*, 2001, **212**, 17–60.
47 M. Rutkowski, D. Wetzig and H. Zacharias, *Phys. Rev. Lett.*, 2001, **87**, 246101.
48 J. J. Mortensen, B. Hammer and J. K. Nøskov, *Surf. Sci.*, 1998, **414**, 315–329.
49 B. Hammer and J. K. Nøskov, *Adv. Catal.*, 2000, **45**, 71–129.

50 L. Y. Gan and Y. J. Zhao, *J. Chem. Phys.*, 2010, **133**, 094703.
51 G. Kresse and J. Hafner, *Phys. Rev. B: Condens. Matter*, 1993, **47**, 558–561.
52 G. Kresse and J. Hafner, *Phys. Rev. B: Condens. Matter*, 1993, **48**, 13115–13118.
53 G. Kresse and J. Furthmuller, *Comput. Mater. Sci.*, 1996, **6**, 15–50.
54 G. Kresse and J. Furthmuller, *Phys. Rev. B: Condens. Matter*, 1996, **54**, 11169–11186.
55 P. E. Blöchl, *Phys. Rev. B: Condens. Matter*, 1994, **50**, 17953.
56 G. Kresse and D. Joubert, *Phys. Rev. B: Condens. Matter Mater. Phys.*, 1999, **59**, 1758.
57 J. P. Perdew and W. Yue, *Phys. Rev. B*, 1986, **33**, 8800.
58 J. P. Perdew, J. A. Chevary, S. H. Vosko, K. A. Jackson, M. R. Pederson, D. J. Singh and C. Fiolhais, *Phys. Rev. B: Condens. Matter*, 1992, **46**, 6671.
59 Test calculations have been carried out using symmetric models (adsorbates on both sides of the slab) in S + NO/Au and NO/Au and NO adsorption energies are 0.47 and 0.35 eV, respectively.
60 H. Aizawa, Y. Morikawa, S. Tsuneyuki, K. Fukutani and T. Ohno, *Surf. Sci.*, 2002, **514**, 394–403.
61 H. R. Tang and B. L. Trout, *J. Phys. Chem. B*, 2005, **109**, 17630–17634, and references therein.
62 W. H. Zhang, Z. Y. Li, Y. Luo and J. L. Yang, *J. Chem. Phys.*, 2008, **129**, 134708.
63 G. Blyholder, *J. Phys. Chem.*, 1964, **68**, 2772.
64 R. Bader, *Atoms in Molecules: A Quantum Theory*, Oxford University Press, New York, 1990.
65 S. J. Jenkins and D. A. King, *Chem. Phys. Lett.*, 1999, **309**, 434–440.
66 J. A. Rodriguez, J. Dvorak, T. Jirsak, G. Liu, J. Hrbek, Y. Aray and C. Gonzalez, *J. Am. Chem. Soc.*, 2003, **125**, 276–285.
67 F. Maca, M. Scheffler and W. Berndt, *Surf. Sci.*, 1985, **160**, 467–474.
68 M. E. Grillo, C. Stampfl and W. Berndt, *Surf. Sci.*, 1994, **317**, 84–98.
69 V. R. Dhanak, A. G. Shard, B. C. C. Cowie and A. Santoni, *Surf. Sci.*, 1998, **410**, 321–329.
70 W. W. Gao, T. A. Baker, L. Zhou, D. S. Pinnaduwage, E. Kaxiras and C. M. Friend, *J. Am. Chem. Soc.*, 2008, **130**, 3560–3565.
71 D. R. Alfonso, *Surf. Sci.*, 2005, **596**, 229–241.
72 M. Todorova, K. Reuter and M. Scheffler, *Phys. Rev. B: Condens. Matter Mater. Phys.*, 2005, **71**, 195403.
73 H. Shi and C. Stampfl, *Phys. Rev. B: Condens. Matter Mater. Phys.*, 2007, **76**, 075327.
74 The computational details of such tests can be found in ref. 50.
75 S. J. Jenkins and D. A. King, *J. Am. Chem. Soc.*, 2000, **122**, 10610–10614.
76 C. Stampfl and M. Scheffler, *Phys. Rev. B: Condens. Matter*, 2002, **65**, 155417.
77 Convergence tests of the vacancy formation energies have been carried out with regard to the K-point sampling and energy cutoff till the total energy difference of each system was less than 0.002 eV.
78 S. K. So, R. Franchy and W. Ho, *J. Chem. Phys.*, 1989, **91**, 5701.
79 K. Nakamoto, *Infrared and Raman Spectra of Inorganic and Coordination Compounds*, Wiley, New York, 1997.